INVESTIGATION OF THE PERFORMANCE OF COLD-END SYSTEM IN DIRECT AIR-COOLED POWER UNITS UNDER THE INFLUENCE OF AMBIENT WINDS

Xingrong ZHU [2], Tingfang YU [*1], Jianyong ZHAN [2], Ying ZHOU [3]

[*1]School of Advanced Manufacturing, Nanchang University, Nanchang, Jiangxi, 330031, China

[2]College of Mechanical and Electrical Engineering, Guangdong University of Science and Technology, Dongguan, Guangdong, 523083, China

[3]Institute of Visual Informatics (IVI), Aras 1, Akademia Siber Teknopolis, Universiti Kebangsaan Malaysia, 43600, Bangi, Selangor

* Corresponding author; E-mail: yutingfang@ncu.edu.cn

Direct air-cooled condensers in power plants rely on heat transfer with the atmospheric environment to discharge thermal energy. The heat transfer process becomes complicated in practical operations when ambient wind is involved. To examine the impact of wind on the heat transfer performance of direct air-cooled condensers, this paper took into consideration three different wind directions, namely, headwind, crosswind and tailwind, as well as four different speeds (3 m/s, 6 m/s, 9 m/s, and 12 m/s), and numerically investigated their influences on the thermal performance of a 600 MW direct air-cooled power unit. The variation in ventilation rates and inlet air temperatures among the cells under the influence of ambient winds are also studied. Simulation results indicated that ambient winds induced thermal air recirculation and air backflow phenomena in the air-cooled island. The cells located on the windward side were significantly affected in all three wind direction conditions. The ventilation rates and inlet air temperatures among the cells were not uniform, showing an overall increasing trend. In particular, negative pressure zones were generated under tailwind conditions, severely impacting air flow rates at the fan inlet, and inlet air temperatures of cells. These phenomena became more pronounced with increasing wind speeds.

Key words*: Direct air-cooled condenser, numerical simulation, ambient wind, heat transfer performance.*

1. Introduction

The condenser, serving both as a heat dissipater and a heat source for steam boilers, holds great significance in the operation of power plants [1]. In the case of direct air-cooled units, the air-cooled condenser is positioned on a platform several meters high, directly exposed to the ambient atmosphere. Consequently, its performance is highly susceptible to the influence of ambient wind. Moreover, the performance of direct air-cooled condensers underwent complex variations during actual operation, as it was affected by multiple factors, including the operating mode of the fans, ambient temperature, and ambient wind speed, all of which interacted with one another [2][3]. The main cooling power source for the cold-end system of direct air-cooled power units was the air-cooled fans. These fans were arranged

in groups within the air-cooled island, and their operational modes significantly impacted the performance of the direct air-cooled power unit [4][5] . The air-cooled fans generated sufficient cooling air through forced ventilation to cool the exhaust steam from the turbine [7]. Klimeš et al. [8] demonstrated through CFD modeling, considering the impact of the fans, that the ventilation rate of the fans affected the heat transfer performance of the direct air-cooled condenser. In the actual operation of air-cooled fans, external environmental conditions, such as ambient wind, could also influence their performance [9][10] thereby affecting the overall performance of the direct air-cooled power unit. As a result, investigating the influence of external ambient wind on the operation of air-cooled fans and their impact on the overall performance of direct air-cooled systems held significant importance.

The direct air-cooled condenser was not only influenced by internal factors such as unit load and steam condensation heat transfer resistance but also by external factors such as ambient wind. Particularly, when the air-cooled island was affected by ambient wind, it was prone to cluster effects, thermal air recirculation, and hot air backflow, which were detrimental to the heat transfer of the air-cooled condenser [11][12]. Currently, numerical simulation methods were widely used to study the impact of ambient wind on the performance of the direct air-cooled cold-end system. Chen et al. [13] conducted numerical simulations on a 600 MW direct air-cooled power unit's air-cooled condenser and found that ambient wind had a significant adverse effect on the heat transfer of the direct air-cooled condenser, hindering the heat transfer efficiency of the air-cooled island. Mahvi et al. [14] considered the influence of steam side pressure drop and thermal resistance, and by establishing a typical model of the direct air-cooled condenser, they demonstrated the necessity of simultaneously considering the negative impact of both steam and ambient wind to improve the performance of the air-cooled condenser. Li et al. [15] studied the effects of changes in the turbine sub-system and environmental conditions on the turbine sub-system and air-cooled condenser of a large-scale air-cooled coal-fired power unit, providing a basis for the safe and economical operation of power plant air-cooled condensers.

Ambient wind conditions included variations in wind direction, wind speed, and wind temperature. It was demonstrated that the air-cooled condenser was influenced by changes in environmental temperature [16][18]. Deng et al. [19], in their research on anti-freezing measures for air-cooled condensers, found that cooling air velocity, ambient temperature, and steam inlet mass flow rate all affected the fin tube wall temperature. The cooling air velocity and temperature that affected the fins of the air-cooled condenser were related to the inlet air velocity and temperature of the air-cooled fans. In reference [20], while considering the backpressure adjustment from the perspective of a single air-cooled condenser unit, it was pointed out that changes in the air flow field and temperature field at inlet of the fan could affect the ventilation rate of the fan, thereby influencing the heat dissipation rate of the air-cooled condenser. Xiao et al. [21], in their study of the thermal-fluid performance of a 300 MW air-cooled combined heat and power unit under the influence of natural winds, indicated that the heat consumption rate of the air-cooled condenser varied with changes in the direction of natural winds. The influence of ambient wind speed and distance between the air-cooled platform and the turbine hall was studied through numerical simulation [21][24]. It was found that under significant ambient wind influence, a compact layout between the air-cooled island and the turbine hall was beneficial in mitigating the impact of ambient wind.

In summary, existing studies concerning the impact of ambient winds on the performance of direct air-cooled condensers were primarily carried out under specific ambient wind conditions. To address

this limitation, this study focused on the heat transfer process of the cold-end system of a 600 MW direct air-cooled power unit, and took into account different wind directions, including headwind, crosswind, and tailwind, as well as varying wind speeds, ranging from 3 m/s, 6 m/s, 9 m/s to 12 m/s.

The remainder of this paper was organized as follows: In Section 2, a numerical model of the cold-end system of a direct air-cooled unit was established. This involved creating a physical model based on the size parameters of the cold-end system (Section 2.1) and dividing it into a computational grid, followed by validation calculations (Section 2.2). In Section 3, introduced the numerical simulation methods. Section 4 set up the numerical simulation boundary conditions by defining the boundaries of the direct air-cooled condenser (Section 4.1), axial flow fans (Section 4.2), and computational domain (Section 4.3). In Section 5, the simulation results were presented and analyzed, with a primary focus on the influence of ambient wind on the flow field and temperature distribution of the air-cooled island when both wind direction and wind speed changed (Section 5.1). To accurately observe the impact of ambient wind on each air-cooled unit, detailed analyses of the variations in airflow rate and inlet air temperature were provided in Sections 5.2 and 5.3, respectively. Finally, Section 6 presented a summary of the research findings.

2. Direct air-cooled power unit cold-end system numerical analysis model

2.1. Physical model of the cold-end system

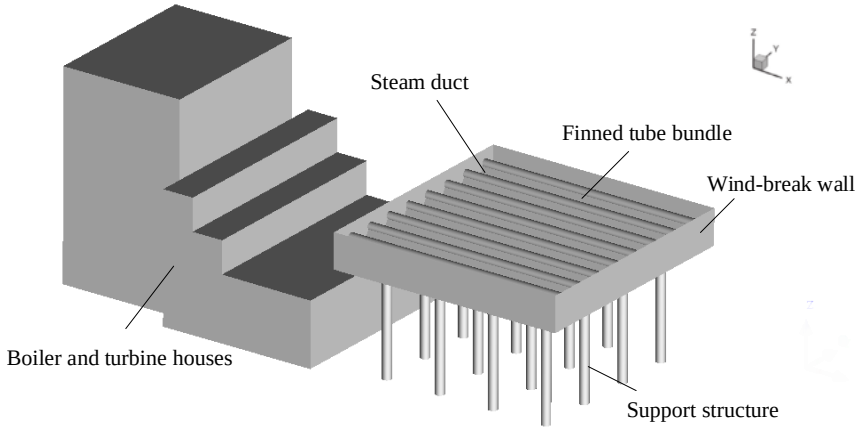

Fig. 1. The physical model of the air-cooled system.

The physical model of the air-cooled system for a specific 600 MW direct air-cooled power unit was illustrated in Figure 1. It included the boiler room, turbine room, and the main equipment, such as the air-cooled condenser, which comprises the steam duct, finned tube bundle, and fans. The air-cooled island was situated adjacent to the turbine room, with a distance of 14 m between them. The dimensions of the boiler room were 71 m in length, 53 m in width, and 87.4 m in height, while the turbine room measured 91.5 m in length, 67 m in width, and 55. 1m in height.

The air-cooled platform comprised 64 air-cooled units arranged in an 8×8 grid, with each unit equipped with an axial-flow fan. The dimensions of the air-cooled platform were 96.8 m in length and 96.6m in width, elevated at a height of 45 m on supporting columns with a diameter of 3.8 m. The spacing between the supporting columns was approximately 24.16 m, with a 2 m-wide aisle on the outside and a 15 m-high windbreak wall. The simulated computational domain had dimensions of 1200 m in length, 800 m in width, and 500 m in height. The air-cooled units were arranged in a "A" shape

with a vertex angle of 60°. The layout and wind directions of the air-cooled units were illustrated in Figure 2.

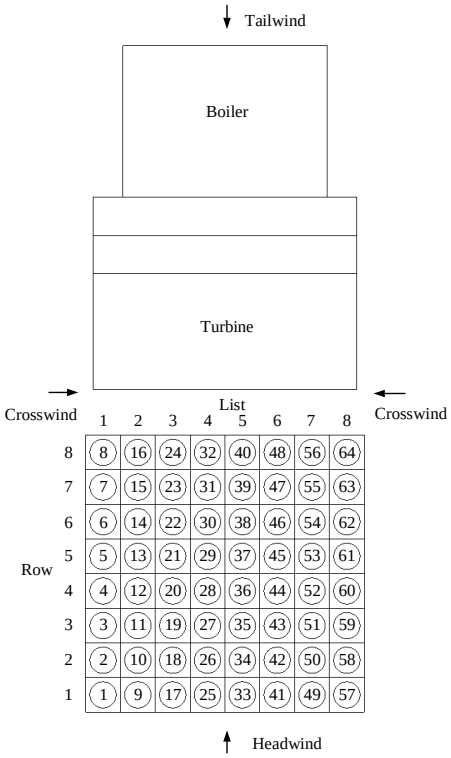

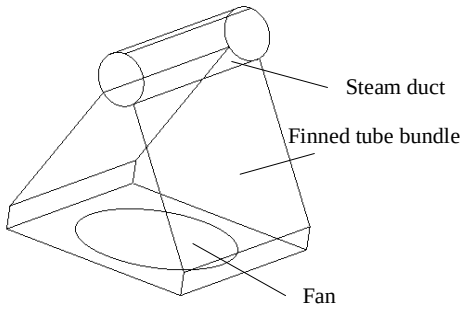

Fig. 2. Air-cooled units and wind directions. **Fig. 3. Simplified diagram of a cell.**

The actual structure of the air-cooled condenser was quite complex, consisting of an array of elliptical finned tubes. Each air-cooled unit also included other auxiliary devices, and the axial-flow fans were composed of blades and hubs. During three-dimensional geometric modeling and FLUENT numerical simulation, the complexity of the radiator and axial-flow fans posed significant challenges in geometric modeling and resulted in a large computational workload. To address this, simplification of the finned tube bundles and fans was necessary.

This study focused on the impact of ambient wind on the inlet air temperature of each air-cooled unit and the performance of the axial-flow fans. The internal airflow characteristics of each air-cooled unit were not the main focus of this research. Therefore, using the lumped parameter approach [25][27], the finned tube bundles and fans of each air-cooled unit could be simplified as an infinitely thin plane, as illustrated in Figure 3.

2.2. Mesh generation and model validation

Given the intricate structure of the direct air-cooled condenser, a hybrid meshing approach was employed. Specifically, the air-cooled island region was meshed using tetrahedral unstructured grids, while the remaining regions were meshed using hexahedral structured grids. To ensure grid independence, three models with mesh sizes of 1,185,823, 1,926,136, and 2,316,104 were evaluated. Figure 4, compared heat transfer rates in the air-cooled condenser under different wind speeds with a headwind direction and an environmental temperature of 20°C. And it was shown that the maximum heat transfer difference among these three mesh sizes was less than 1%. Consequently, the model employing 1,926,136 grid cells was selected for subsequent calculations.

Figure 5 illustrates the simulation results of air-cooled unit backpressure using the backpressure calculation method proposed in reference [31], in conjunction with the numerical model established in this study. These results were compared with corresponding actual backpressure values, revealing a close alignment between the simulated and actual values, with a maximum error of less than 1.8%. This validation attests to the reliability of the numerical model.

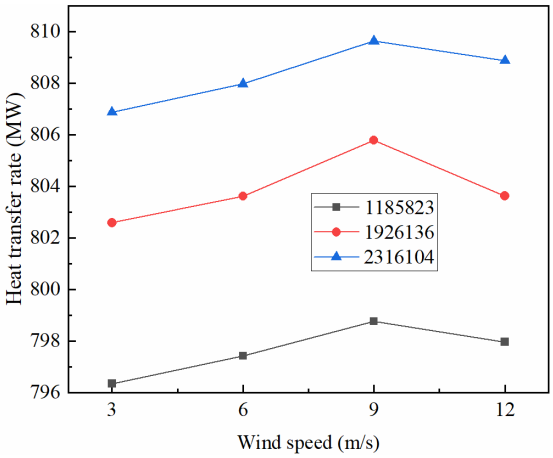

Fig. 4. Air-cooled condenser heat transfer rate under different wind speeds.

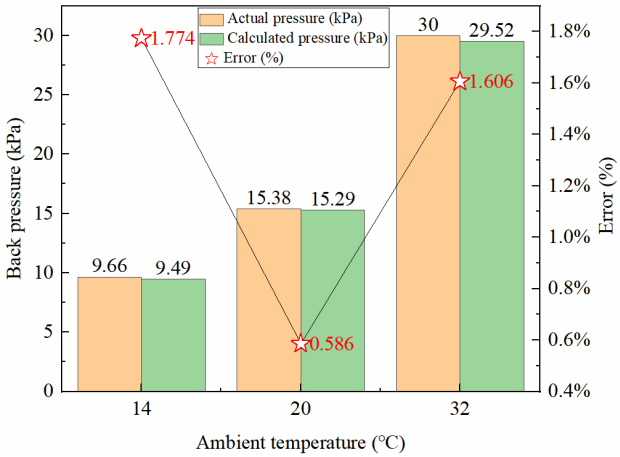

Fig. 5. Comparison of unit back pressure between simulated and actual values.

3. Calculation method

In this study, the FLUENT software was used for numerical simulations of the cold-end system in the direct air-cooled power plant. The numerical calculations were based on the SIMPLE algorithm, and the standard k-ε model was employed for turbulent flow calculations. Due to the complexity of air flow, the air was assumed to be an incompressible ideal fluid with heat transfer. Therefore, the governing equations involved in the solution process included the continuity equation, momentum conservation equation, and energy conservation equation. The k-ε model included the turbulent kinetic energy equation and the turbulent dissipation rate equation. The detailed expressions could be found in the references [7][27], and they were not reiterated here.

4. Boundary conditions

4.1. Direct air-cooled condenser settings

The direct air-cooled condenser exchanged heat with the external air through its finned tube bundle. To simplify the complex heat exchange process of the finned tube bundle, it was approximated as an infinitely thin plane using the Radiator model. The numerical simulation of the direct air-cooled condenser was achieved by setting corresponding resistance coefficients, heat transfer coefficients, and temperature parameters.

In the Radiator model, the pressure drop Δp across the finned tube bundle was related to the normal velocity v perpendicular to the surface of the finned tube bundle through a specific function, expressed as:

$$\Delta p = \frac{1}{2} k_L \rho v^2 \tag{1}$$

where k_L was the dimensionless loss coefficient, represented using a polynomial function:

$$k_L = \sum_{n=1}^{N} r_n v^{n-1} \tag{2}$$

where the coefficients r_n were the polynomial fitting coefficients, which were obtained through curve fitting experiments [25]. In this paper, N was taken as 3, r_1=71.6888, r_2= -31.7074, r_3=13982.

The heat absorbed by the air when flowing through the finned tube bundle was given by:

$$q = h\left(T_s - T_a\right) \tag{3}$$

where T_s (°C) represented the steam condensation temperature in the air-cooled condenser. Since the heat resistance from steam condensation inside the radiator tubes was very small, and the tube wall was thin with a relatively high thermal conductivity, heat resistance from steam condensation inside the tubes and heat conduction through the tube wall can be neglected. As a result, the steam condensation temperature was equal to the saturation temperature at the pressure of the condenser. T_a (°C) was the downstream air temperature of the radiator, and h was the convective heat transfer coefficient.

The convective heat transfer coefficient (h) could be represented using a polynomial as follows:

$$h = \sum_{n=1}^{N} h_n v^{n-1} \tag{4}$$

where the convective heat transfer polynomial coefficients denoted as h_n were calculated through curve fitting in a manner similar to the polynomial coefficients r_n [25]. In this case, the value of N was set to 3, h_1=536.993, h_2=2016.0887, h_3= -97.7721.

4.2. Axial flow fan configuration

In this study, the axial flow fan was treated as an infinite thin surface using the lumped parameter approach. The fan model was determined by inputting the fan performance curve, which related the fan static pressure to the normal velocity of the fluid flowing through the fan. The relationship between the fan static pressure and the normal velocity was expressed as follows:

$$\Delta p = \sum_{n=1}^{N} f_n v^{n-1} \tag{5}$$

where Δp (Pa) represented the pressure increment of the fan, f_n were the polynomial coefficients, and v (m/s) represented the normal velocity of the fluid passing through the fan.

Based on the operating data of the fan, the relationship between fan static pressure and normal velocity could be obtained. The design parameters of the fan in this study were shown in Table 1.

Tab.1 Fan design parameters.

Diameter(m)	Speed (rpm)	Airflow Rate(m^3/s)	Motor Power(KW)	Total Pressure(Pa)
9.144	69	469	110	93

According to the performance curve of the air-cooled fan [28], the least squares method was applied to fit the fan parameters and fan performance parameters to obtain the relationship between fan static pressure and axial velocity. The resulting curve was shown in Figure 6, where "n" represented the rated fan speed.

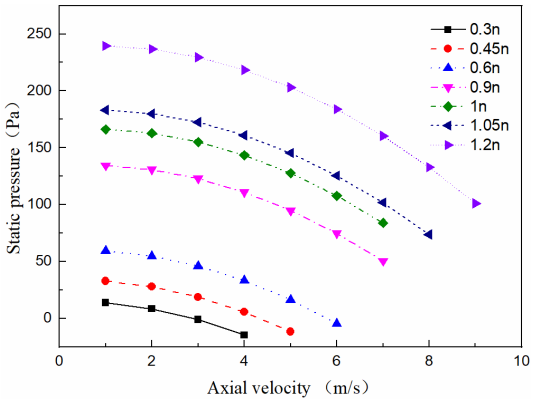

Fig. 6. Fitting curve of the static pressure and the axial velocity of the fan.

4.3. Other boundary conditions setting

Under the influence of ambient wind, the wind speed varies at different heights, and the ambient wind speed generally increases with increasing height. When setting the velocity boundary conditions at the inlet, a user-defined function (UDF) was utilized along with a programmed approach for calculation. The functional relationship between the ambient wind speed and the height was described by the following expression [29][30]:

$$v_i = v_{10}\left(\frac{z_i}{10}\right)^m \tag{6}$$

where v_{10} (m/s) was the wind speed at a height of 10 meters above the ground, z_i (m) was the height at any arbitrary location, v_i (m/s) was the wind speed at the height z_i, m was the ground roughness coefficient, and in this study, its value was taken as 0.16.

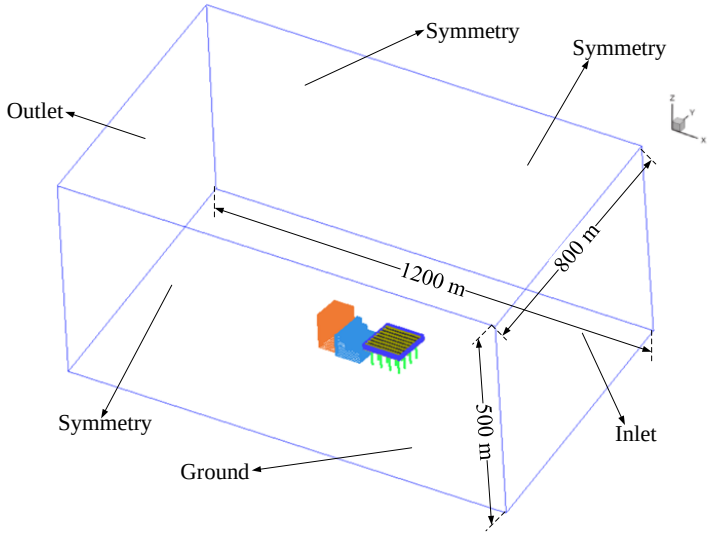

Fig. 7. Direct air-cooled system computational domain and its boundary conditions.

A more detailed description of the modeling process and simulation calculations for the direct air-cooled condenser system, and the boundary conditions for the windward face, outlet, and other boundaries of the computational domain is referred to [31]. Figure 7 showed the schematic diagram of the computational domain and boundary conditions for the direct air-cooled system under headwind

conditions. For other wind directions, only the positions of the inlet and outlet boundaries needed to be adjusted, while the other boundary conditions remained unchanged.

5. Results and analysis

This study investigated the impact of different wind directions (headwind, crosswind, and tailwind) and various ambient wind speeds (3 m/s, 6 m/s, 9 m/s and 12 m/s) on the heat transfer performance of the air-cooling system. The simulations were conducted at an ambient temperature of 20 °C, rated load of the unit, and rated speed of the fan.

5.1. Impact of ambient wind on flow and temperature

5.1.1 The headwind impact

In Figure 8, under headwind conditions at different wind speeds, the temperature and airflow patterns in the direct air-cooled island were observed. Air entered the island head-on and passed through axial flow fans, exchanging heat in finned tubes with steam inside condenser tubes. The heated air was then carried over the island's top by the wind, forming a thermal wake. The airflow patterns and temperature distribution revealed deformations near the boiler and turbine areas, forming vortices between the air-cooled platform and these regions. With increasing wind speed, the thermal wake lowered, and the vortex area expanded. Strong vortices, coupled with the axial flow fans' suction, caused hot air to flow back between the air-cooled condenser and the boiler/turbine area.

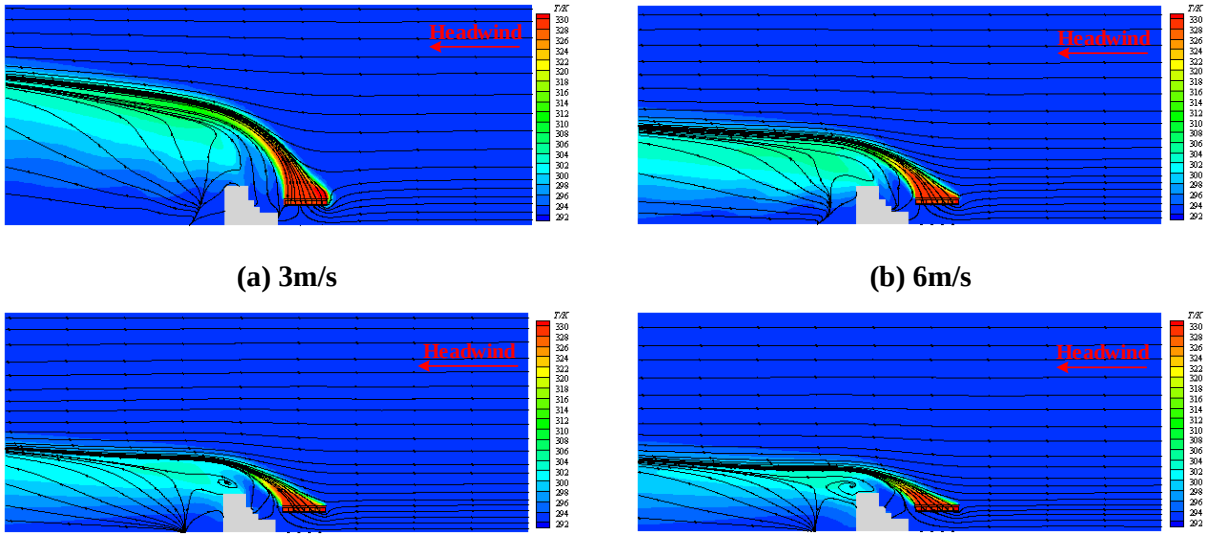

(a) 3m/s **(b) 6m/s**

(c) 9m/s **(d) 12m/s**

Fig. 8. Streamline and temperature contour under headwind.

5.1.2 The crosswind impact

Figure 9, shows airflow and temperature patterns within the air-cooled island under crosswind conditions at varying speeds. Higher wind speeds reduced the flow of hot air above the air-cooled condenser, worsening heat dissipation. Crosswinds caused backflow in edge air-cooled units, intensifying with wind speed. Wind significantly affected axial fans on the windward side, impacting more units at higher speeds (12 m/s affecting nearly all eight rows).

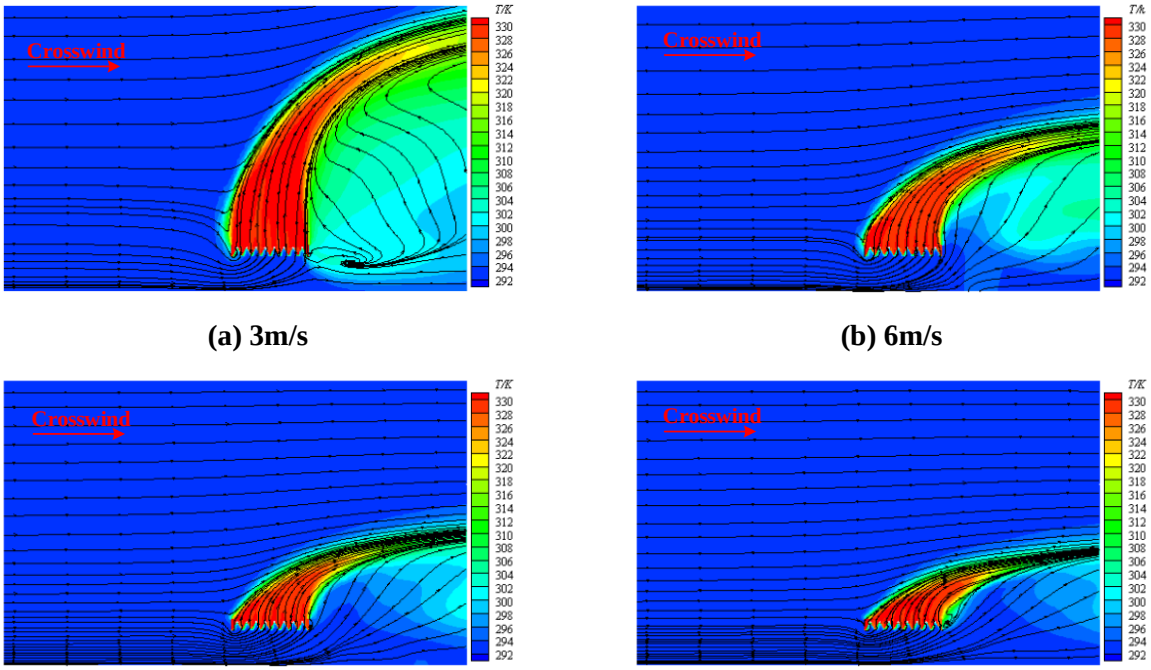

(a) 3m/s **(b) 6m/s**

(c) 9m/s **(d) 12m/s**

Fig. 9. Streamline and temperature contour under crosswind.

5.1.3 The tailwind impact

Figure 10 illustrates the impact of tailwind on the air-cooled island, showing airflow patterns and temperature at different speeds. Tailwinds created vortex zones between the air-cooled platform, boiler, turbine room, and behind the windbreak wall, causing thermal backflow drawn by axial fans. Faster tailwinds intensified negative pressure between the air-cooled platform and the boiler/turbine room, worsening thermal backflow and affecting more units. Tailwinds absorbed heat from the boiler/turbine rooms, causing lower heat transfer performance than headwind or crosswind conditions.

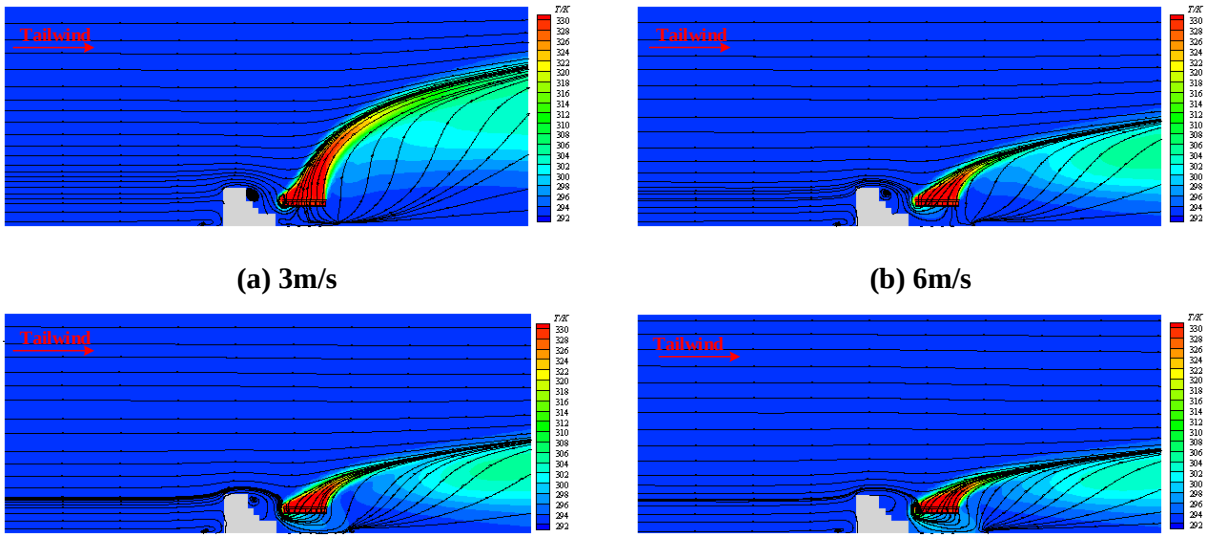

(a) 3m/s **(b) 6m/s**

(c) 9m/s **(d) 12m/s**

Fig. 10. Streamline and temperature contour under tailwind.

5.2. Impact of ambient wind on airflow rate in air-cooled cells

To better understand the impact of ambient wind on each air-cooled cell, the airflow rate and inlet air temperature of the direct air-cooled condenser cells were studied and analyzed under varying ambient wind directions and speeds.

5.2.1 The impact of headwind

Analysis of airflow rates in the direct air-cooled island under headwind conditions and the variation patterns of the air-cooled units at different ambient wind speeds were shown in Figure 11.

In Figure 11(a), the airflow rates of each air-cooled unit at a 3 m/s ambient wind speed were shown. Despite uniform axial fan speeds, actual airflow rates varied. The first-row units, exposed to headwinds and strong ambient wind interference, had the lowest airflow rates due to larger negative pressure zones at their inlets. This reduced the axial fan's air intake, resulting in lower airflow rates. As we move beyond the first row, airflow rates gradually increased as the influence of headwinds diminished, allowing smoother air intake and higher rates.

Figure 11(b) displayed airflow rate variations for middle-column air-cooled units under various ambient wind speeds. Higher wind speeds particularly affected air-cooled units in the headwind region. The first two rows experienced significant decreases in airflow rates, while downstream units were less affected, sometimes even surpassing design values. This was primarily due to increased wind speeds disrupting the flow field around the second-row units' inlets, making it harder for air to enter the fan inlet. As wind speed increased, the negative pressure area under the headwind units expanded, causing a greater reduction in airflow rates for the second-row units.

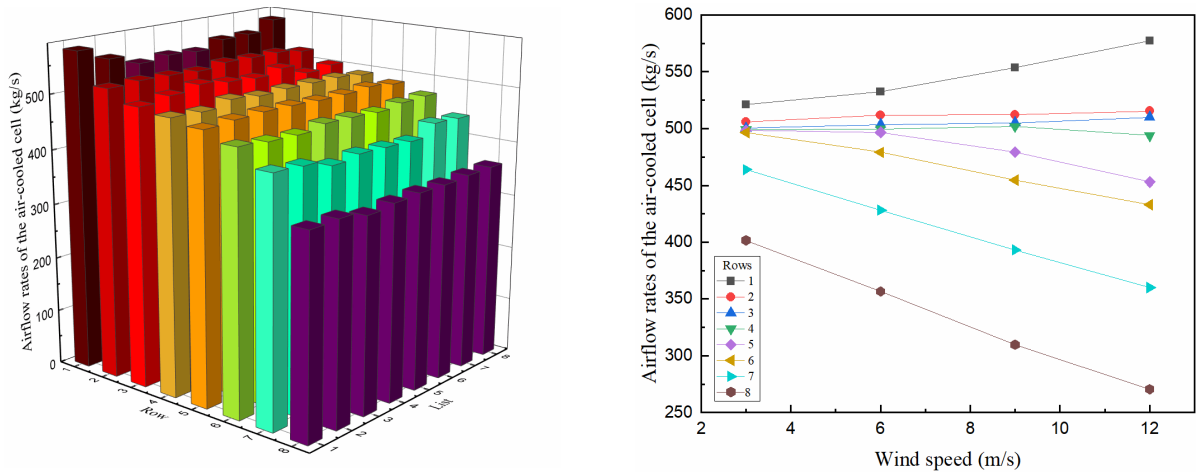

(a) Airflow rates of each air-cooled cell **(b) Airflow rates vs. wind Speed**

Fig. 11. The impact of headwind on the airflow rates of the air-cooled cells.

5.2.2 The impact of crosswind and tailwind

Under crosswind and tailwind conditions, the airflow rates of each air-cooled unit in the direct air-cooled island, along with their variations at different ambient wind speeds, were presented in Figure 12 and Figure 13, respectively. As shown in Figure 12(a) and Figure 13(a), the impact of ambient wind on the airflow rates of each air-cooled unit under crosswind and tailwind conditions was similar to that

under headwind conditions. The actual airflow rates of the air-cooled units also varied, with the first row having the lowest airflow rate, and the airflow rates gradually increasing from the second to the eighth row. In Figure 12(b) and Figure 13(b), it could be observed that the effect of different ambient wind speeds on the airflow rate of the middle-row air-cooled units was similar to that under headwind conditions. However, under tailwind conditions, the first-row air-cooled unit in the headwind region was more affected by the ambient wind compared to the other rows. This was mainly due to the more direct influence of the vortex region between the air-cooled platform and the boiler and turbine room, leading to a more severe heat recirculation under tailwind conditions.

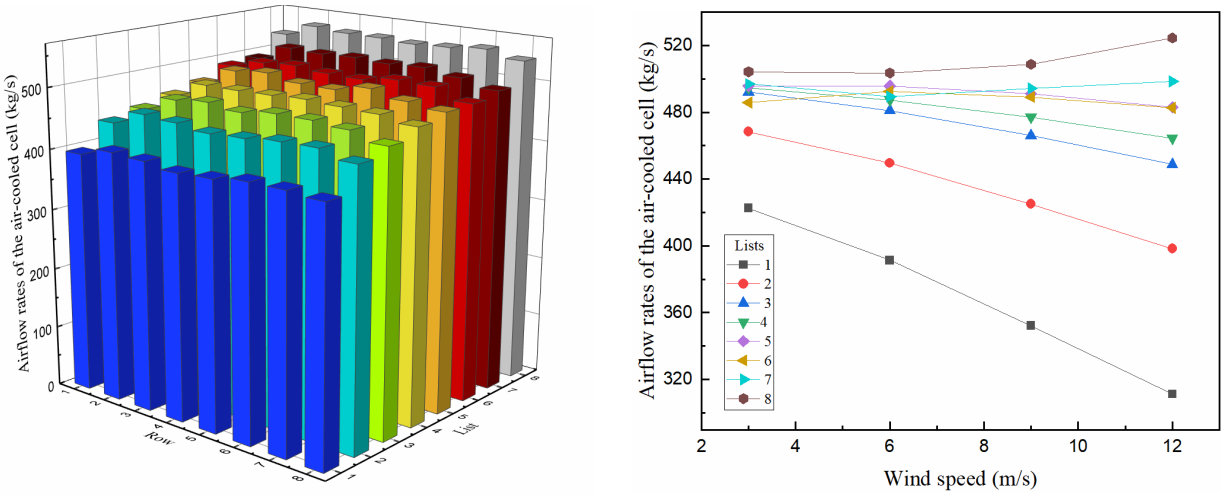

(a) Airflow rates of each air-cooled cell **(b) Airflow rates vs. wind Speed**

Fig. 12. The impact of crosswind on the airflow rates of the air-cooled cells.

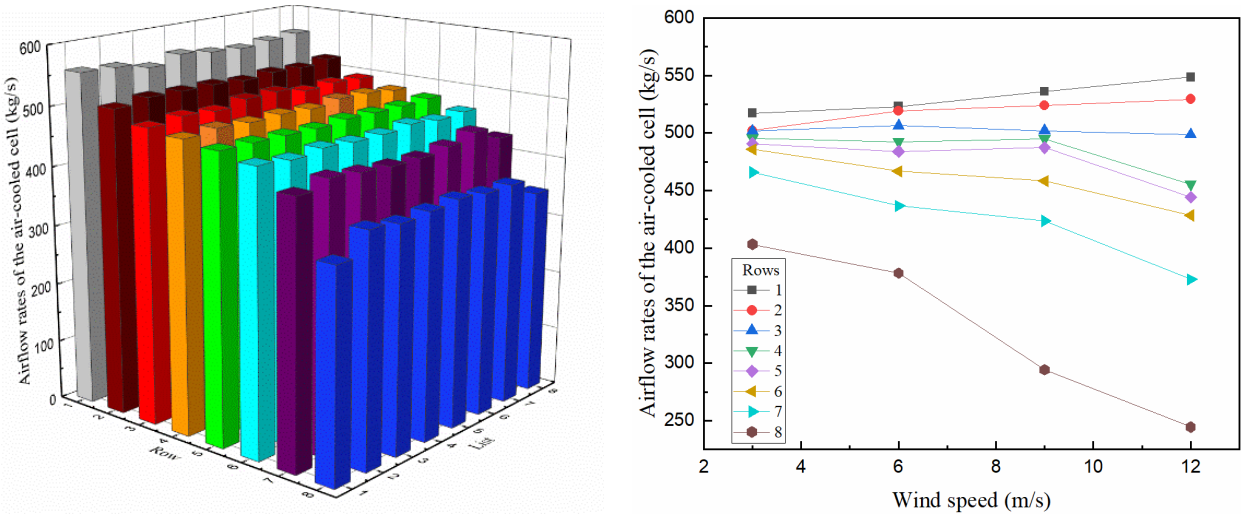

(a) Airflow rates of each air-cooled cell **(b) Airflow rates vs. wind Speed**

Fig. 13. The impact of tailwind on the airflow rates of the air-cooled cells.

5.3. Impact of ambient wind on the inlet temperature of air-cooled cell

5.3.1 The impact of headwind

In Figure 14(a), under a 3 m/s headwind, the inlet air temperature of each air-cooled unit varied. The first-row unit had the lowest inlet air temperature, gradually rising as we moved away from the headwind. In the edge region, the inlet air temperature was notably higher. This was because the first-row unit was minimally affected by the ambient wind, keeping its inlet air temperature close to the environment. In contrast, downstream units experienced increased ambient wind-induced hot air recirculation, raising their inlet air temperatures. Edge units experienced larger negative pressure areas due to significant hot air recirculation, leading to even higher inlet air temperatures.

In Figure 14(b), showing inlet air temperatures of edge column air-cooled units under headwind conditions with varying wind speeds, as the distance from the headwind increased, inlet air temperatures gradually rose. For the same unit, higher ambient wind speeds led to lower inlet air temperatures. The first and second-row units were less affected by wind speed changes and remained close to environmental air temperature. However, at a wind speed of 3 m/s, the eighth-row unit had the highest inlet air temperature. At 6 m/s, the seventh and eighth-row units had the highest inlet air temperatures. At 9 m/s and 12 m/s, the sixth, seventh, and eighth-row units had similar and relatively high inlet air temperatures. This was related to stronger wind speeds impacting edge units, causing lower fan inlet air temperatures due to hot air recirculation. The first and second-row units, located in the headwind region, remained minimally affected, with their inlet air temperatures close to the environment. However, at a wind speed of 3 m/s, the eighth-row unit experienced significant hot air recirculation. As wind speed increased, this phenomenon became more severe, affecting more units near the boiler and turbine rooms. Consequently, at 6 m/s, not only the eighth-row unit but also the adjacent seventh-row unit were affected. With wind speeds of 9 m/s and 12 m/s, even the sixth-row unit, near the boiler and turbine rooms, had higher inlet air temperatures due to hot air recirculation.

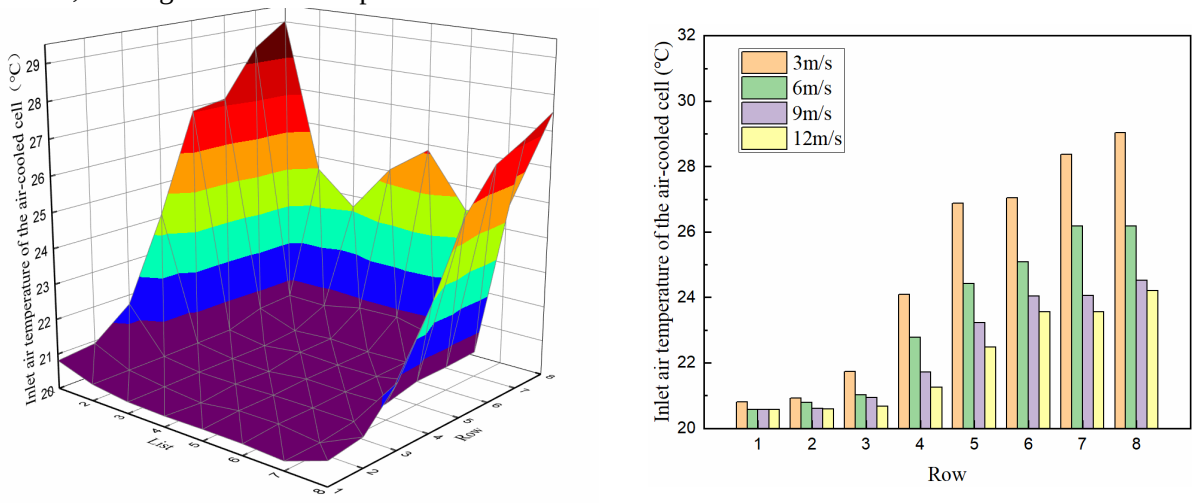

(a) Inlet temperature of each air-cooled cell **(b) Inlet air temperature vs. wind Speed**

Fig. 14. The impact of headwind on the inlet air temperature of the air-cooled cells.

5.3.2 The impact of crosswind

In Figure 15(a), under 3 m/s crosswind conditions, the inlet air temperatures of each air-cooled unit varied. Similar to headwind conditions, crosswinds affected inlet air temperatures differently across units. Units in the headwind region were less affected, with inlet air temperatures closest to the environment. Moving away from the headwind, inlet air temperatures increased, and edge units had notably higher temperatures compared to middle units.

Figure 15(b) displayed inlet air temperatures of edge units at different wind speeds under crosswind conditions. Similar to headwinds, inlet air temperatures increased with distance from the headwind. For the same unit, higher wind speeds resulted in lower inlet air temperatures. Downstream edge units had higher inlet air temperatures than upstream units due to crosswind-induced hot air backflow. However, compared to headwind and tailwind scenarios, the crosswind-induced backflow had a smaller impact on downstream edge units' inlet air temperatures than the hot air recirculation caused by vortex phenomena near the boiler and turbine rooms.

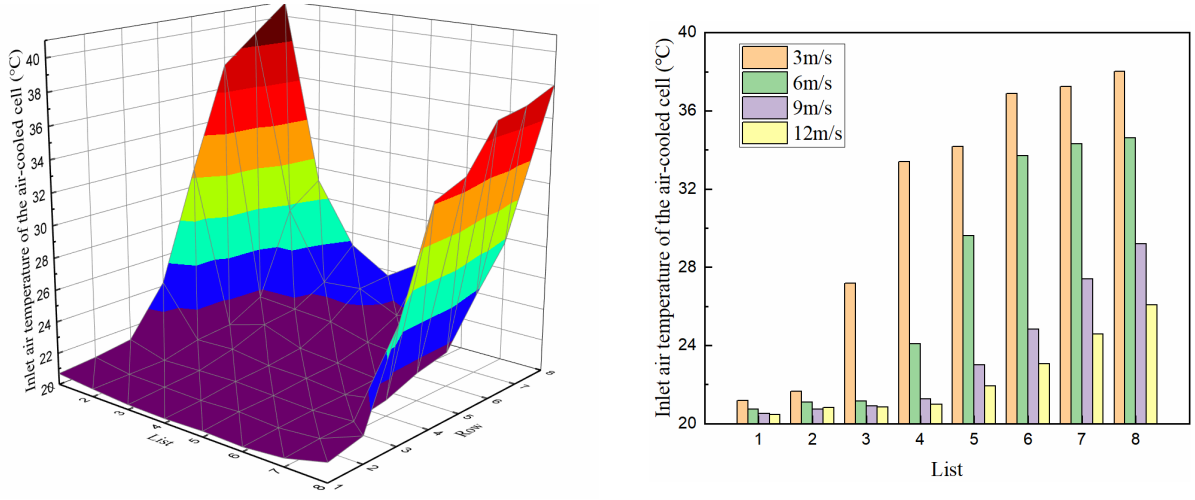

(a) Inlet temperature of each air-cooled cell **(b) Inlet air temperature vs. wind Speed**

Fig. 15. The impact of crosswind on the inlet air temperature of the air-cooled cells.

5.3.3. The impact of tailwind

In Figure 16(a), at a 3 m/s tailwind, the air-cooled unit inlet temperatures differed notably from headwind and crosswind scenarios. Edge units had higher temperatures than those in the middle. Importantly, inlet temperatures increased row by row from the seventh to the first. Surprisingly, the eighth-row unit at the headwind edge had a higher temperature than the subsequent seventh-row unit, contrasting headwind and crosswind scenarios where the headwind's first-row unit had the lowest temperature.

Specifically, the eighth-row unit in the middle, close to the boiler and turbine rooms, experienced local negative pressure, forming vortices causing hot air backflow and elevated temperatures. Edge units on both sides were less affected, while the middle region had higher negative pressure and more backflow.

In Figure 16(b), a similar trend emerged at varying wind speeds. Inlet temperatures increased with distance from the tailwind, and higher wind speeds reduced inlet temperatures for each unit.

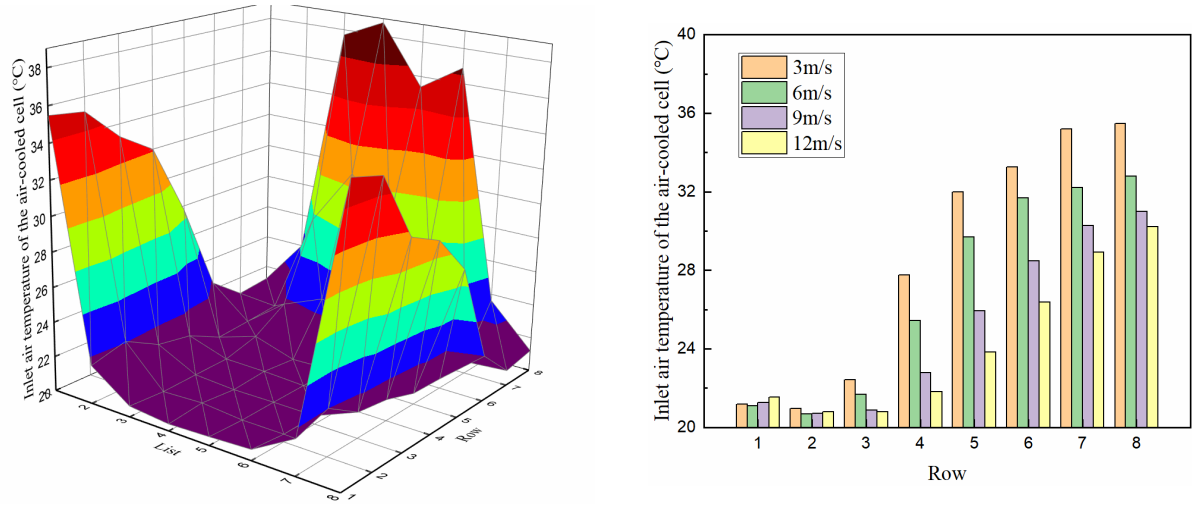

(a) Inlet temperature of each air-cooled cell **(b) Inlet air temperature vs. wind Speed**

Fig.16. The impact of tailwind on the inlet air temperature of the air-cooled cells

6. Conclusion

This study created a numerical model for a 600 MW direct air-cooled unit's cooling system, investigating its heat transfer performance in varying winds. The findings can be summarized as follows:

1. Air-cooled units near boiler and turbine areas experience hot air backflow, especially in crosswinds, which intensifies with higher wind speeds.

2. Windward-side units are more affected, with greater impact at higher wind speeds. Tailwinds create the largest negative pressure zone, significantly affecting fan airflow.

3. Ventilation rates and inlet air temperatures vary with wind direction. Ventilation rates increase gradually from the first to the last row. Higher wind speeds notably reduce ventilation in the first two windward rows, but less so in downstream units.

4. Under headwind and crosswind, windward-side units have the lowest inlet air temperature, gradually increasing downstream. In tailwinds, apart from the first-row edge unit, others also see rising inlet temperatures. Edge units have notably higher inlet temperatures than the middle. All units' inlet air temperatures decrease with higher wind speeds, with more impact on units near the boiler and turbine rooms.

In summary, the research demonstrates that ambient wind can indeed impact air-cooled units as wind speed and direction change. For future investigations, measures such as windbreak nets and deflectors will be incorporated into numerical modeling to reduce the influence of ambient wind, especially those originating from the tailwind of the furnace, which tend to have the most significant effect.

While the current study focused on headwind, crosswind, and tailwind conditions, it's important to note that ambient wind is continuously variable. Therefore, future research will also explore the effects of changing wind directions by subdividing wind directions into a 0° to 360° range. This approach will enable a more detailed and comprehensive analysis of their impacts on the air-cooled island.

References

[1] Lakovic, M., *et al*., Impact of the cold end operating conditions on energy efficiency of the steam power plants, *Thermal Science, 14* (2010), suppl., pp. 53-66

[2] Li, X., *et al*., A data-driven model for the air-cooling condenser of thermal power plants based on data reconciliation and support vector regression, *Applied Thermal Engineering, 129* (2018), pp. 1496-1507

[3] Lin, X., *et al*., Cold-end integration of thermal system in a 1000 MW ultra-supercritical double reheat power plant, *Applied Thermal Engineering, 193* (2021), pp. 116982

[4] Luo Z., *et al*., Energy-efficient operation of a direct air-cooled condenser based on divisional regulation, *International Journal of Refrigeration, 132* (2021), pp. 233-242

[5] Yang, T., *et al*., Closed-loop optimization control on fan speed of air-cooled steam condenser units for energy saving and rapid load regulation, *Energy, 135* (2017), pp. 394-404

[6] Zhu M., *et al*., Dynamic modeling, validation and analysis of direct air-cooling condenser with integration to the coal-fired power plant for flexible operation, *Energy Conversion and Management, 245* (2021), pp. 114601

[7] He, W. F., *et al*., Performance prediction of an air-cooled steam condenser using UDF method, *Applied Thermal Engineering, 50* (2013), 1, pp. 1339-1350

[8] Klimeš, L., *et al*., Semi-empirical balance-based computational model of air-cooled condensers with the A-frame layout, *Energy, 182* (2019), pp.1013-1027

[9] Deng, H. Liu, J. Performance Prediction of Finned Air-Cooled Condenser Using a Conjugate Heat-Transfer Model, *Applied Thermal Engineering, 150* (2019), pp. 386–397

[10] Zhang, Y., *et al*., Dynamic modeling and control of direct air-cooling condenser pressure considering couplings with adjacent systems, *Energy, 236* (2021), pp. 121487

[11] Zheng, G., *et al*., Cluster Partition Operation Study of Air-Cooled Fan Groups in a Natural Wind Disturbance, *Energies, 16* (2023), 9, pp. 3717

[12] Gao, X. F., *et al*., Performance prediction of an improved air-cooled steam condenser with deflector under strong wind, *Applied Thermal Engineering, 30* (2010), 17, pp. 2663-2669

[13] Chen, L., *et al*., A novel layout of air-cooled condensers to improve thermo-flow performances, *Applied Energy, 165* (2016), 165, pp. 244-259

[14] Mahvi, A. J., *et al*., Challenges in predicting steam-side pressure drop and heat transfer in air-cooled power plant condensers, *Applied Thermal Engineering, 133* (2018), pp. 396-406

[15] Li, X. E., *et al*., Identification of optimal operating strategy of direct air-cooling condenser for Rankine cycle based power plants, *Applied Energy, 209* (2018), 153, pp. 153-166

[16] Jin, Y., *et al*., Analysis of joint operation of air-cooling system and peak cooling device in summer, *Applied Thermal Engineering, 188* (2021), pp. 116635

[17] Pieve, M., Salvadori. G., Performance of an air-cooled steam condenser for a waste-to-energy plant over its whole operating range, *Energy Conversion and Management, 52* (2011), 4, pp. 1908-1913

[18] Feng, P., Luo, Z., Back pressure optimization of direct air-cooled condenser considering anti-freezing and low-load operation, *IOP Conference Series: Materials Science and Engineering, 569* (2019), pp. 032029-

[19] Deng, H., *et al*., Numerical investigation on complete condensation and freezing of finned tube air-cooled condensers, *Applied Thermal Engineering, 168* (2020), 5, pp.114428

[20] Li, J., *et al*., Operation of air cooled condensers for optimised back pressure at ambient wind, *Applied Thermal Engineering, 128* (2018), pp. 1340-1350

[21] Xiao, L., *et al*., Operation of air-cooling CHP generating unit under the effect of natural wind, *Applied Thermal Engineering, 107* (2016), pp. 827-836

[22] Xiao, L., *et al*., Air-cooling condenser layout of 2×1000MW direct air-cooled units under effect of ambient natural wind, *Electric Power Construction, 36* (2015), 6, pp. 7-13 (in Chinese)

[23] Luo, Z., Yao, Q., Multi-Model-Based Predictive Control for Divisional Regulation in the Direct Air-Cooling Condenser, *Energies, 15* (2022), 13, pp. 4803

[24] Ma, H., *et al*., Numerical study identifies the interaction between two adjacent dry cooling towers on fluid flow and heat transfer performances of the radiators at different points of each tower, *International Journal of Thermal Sciences, 191* (2023), pp. 108351

[25] Yang, L., *et al*., Numerical investigation on the cluster effect of an array of axial flow fans for air-cooled condensers in a power plant, *Chinese Sci Bull, 56* (2011), 21, pp. 2272-2280 (in Chinese)

[26] Yang, L. J., *et al*., Space characteristics of the thermal performance for air-cooled condensers at ambient winds, *International Journal of Heat and Mass Transfer, 54* (2011), 15, pp. 3109-3119

[27] Li, M., *et al*., Correction algorithm for calculating heat transfer in air-cooling condenser based on analyzing steam condensation locations, *Energy Sources, Part A: Recovery, Utilization, and Environmental Effects, 45* (2023), 3, pp. 6744-6755

[28] Hu, H., Research on flow and heat transfer of finned heat exchanger of direct-cooled condenser and flow characteristic of condenser unit, M.S. thesis, Chongqing University, Chongqing , CHN, 2006

[29] Chen, L., *et al*., Rotational speed adjustment of axial flow fans to maximize net power output for direct dry cooling power generating units, *Heat Transfer-Asian Research, 49* (2020), 1, pp. 356-382

[30] Chen, L., *et al*., Subregional modulation of axial flow fans to reduce condensate supercooling of air-cooled steam condenser in cold days, *Applied Thermal Engineering, 193* (2021), pp. 117016

[31] Zhu, X., Zhan, J., Operation optimization of cold-end system of direct air-cooled units considering the effect of environmental wind, *Heat Transfer, 52* (2023), 06, pp. 4337-4356

Submitted: 09.06.2023.
Revised: 20.09.2023.
Accepted: 30.11.2023.